

pubs.acs.org/Macromolecules Article

# Impact of Side-Chain Length on the Self-Assembly of Linear-Bottlebrush Diblock Copolymers

Lucy Liberman, McKenzie L. Coughlin, Steven Weigand, Jerrick Edmund, Frank S. Bates, and Timothy P. Lodge\*



**Cite This:** *Macromolecules* 2022, 55, 4947–4955



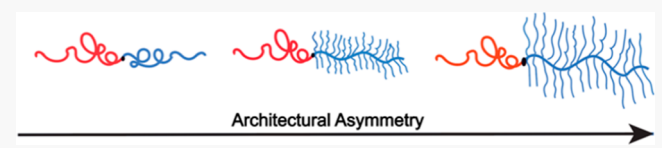
**ACCESS** 

Metrics & More



Supporting Information

**ABSTRACT:** Diblock polymers are known to self-assemble into a variety of structures, and the effects of block molecular weights and volume fractions, along with the interactions between chemically different blocks, have been extensively studied. However, the consequences of molecular architectural differences between the blocks on phase behavior, particularly self-assembly into network



morphologies, are less well explored. In this work, 223 linear-bottlebrush diblock polymers were synthesized using grafting-through living ring-opening metathesis polymerization. The linear block was poly(norbornene exo,exo-dimethyl ester), while five different bottlebrush blocks were used in order of increasing side-chain length: poly(norbornene exo,exo-di-isoamyl ester), poly(norbornene exo,exo-di-3,7-dimethyloctyl ester), poly(norbornene exo,exo-di-hexahydrofarnesyl ester), poly(norbornene exo,exo-di-dihydrophytyl ester), and poly(norbornene exo,exo-di-perhydrosolanesyl ester). Diblock polymer compositions ranged from approximately 30 to 70% by volume of the linear block, with total backbone degrees of polymerization ranging from 30 to 140, and side chains containing 5–45 carbon atoms. Phase behavior was studied in the vicinity of the double gyroid network window using a combination of small-, mid-, and wide-angle X-ray scattering.

#### **■ INTRODUCTION**

Self-assembly of diblock polymers into ordered network phases such as the double gyroid, double diamond, and orthorhombic *Fddd* (O<sup>70</sup>) has attracted much interest, in particular due to the many promising applications enabled by the percolating domains.<sup>1–7</sup> In linear diblock polymers, the accessible region for network phase formation is limited to a narrow range of volume fractions due to the high packing frustration of polymer blocks at the multi-node connectors, as demonstrated by experiments and self-consistent field theory (SCFT).<sup>8–10</sup> Another practical limitation is the slow ordering kinetics of high-molecular-weight linear diblocks, which can inhibit self-assembly into network phases. This places a practical upper limit on the accessible network domain size, thereby limiting the range of practical applications.

Previous SCFT and experimental studies suggest that the introduction of architectural asymmetry into a diblock polymer induces spontaneous curvature at the interface between the domains, which could relieve the packing frustration associated with complex phases. One way to tune the architectural asymmetry is by the incorporation of a bottlebrush polymer as one of the blocks. The polymer shape and the transition from a Gaussian coil to a wormlike chain are controlled by the backbone and side-chain lengths and the grafting density. Precise control over the architecture is enabled by recent advances in controlled polymerization techniques, such as ringopening metathesis polymerization (ROMP). Here, using ROMP as a platform, we design block polymers with

systematically increasing architectural asymmetry. Through changes in the side-chain length of one of the blocks, we study how the transition from a linear-linear to a linear-brush configuration affects the diblock phase behavior in the vicinity of network formation.

Most prior SCFT and experimental work on linear-brush and linear-comb diblock polymers primarily focused on the formation of complex sphere phases, lamellae, and cylinders. 12,20–27 However, a recent SCFT study by Park et al. 13 predicts a double gyroid stability window for linear-brush diblock polymers. Moreover, this work also reports that this window shifts to higher compositions with the increase in sidechain length of the brush block, that is, increasing architectural asymmetry. 13 This trend is in agreement with previous theoretical predictions in other architecturally asymmetric diblock polymer systems. 11,14,15 In our recent work dealing with the phase behavior of linear-brush polymers, we synthesized eight sets of polymers (a total of 258 polymers), and systematically studied the consequences of varying the length of the linear block and the side-chain length of the brush block. 28 Focusing on the double-gyroid region, we

Received: April 13, 2022 Revised: May 27, 2022 Published: June 14, 2022





demonstrated that the increase in the side-chain length of the brush, which increases the architectural asymmetry, shifts the phase boundaries toward higher linear block compositions, in agreement with the theoretical predictions. Furthermore, the difference in cohesive energy density between the linear and brush blocks was shown to influence the order—disorder transition (ODT) and the size of the gyroid compositional window.<sup>28</sup>

In this work, we prepared five series of norbornene-based diblock polymers with increasing side-chain length of the bottlebrush block to gain a more complete understanding of the effect of architectural asymmetry on the phase behavior in the proximity of the gyroid window. Using ROMP, we varied with high precision the compositions and the degree of polymerization of a total of 223 individual block polymers. Using mid-angle X-ray scattering (MAXS), we studied how the side-chain length affects the transition from a linear-linear to a linear-brush configuration. Small-angle X-ray scattering (SAXS) measurements provide for a comprehensive characterization of how increasing architectural asymmetry affects the phase boundaries, phase coexistence, interaction parameter, and the size of the double-gyroid compositional window.

#### EXPERIMENTAL SECTION

**Materials.** Solanesol was purchased from Cayman Chemical Company as a yellow powder and was dissolved in benzene, filtered, and lyophilized for purification; cis-5-norbornene-2,3-dicarboxylic anhydride was purchased from TCI Chemicals; phytol was acquired from ApexBio; SiliaMetS [SiliCycle Inc SiliaBond dimercaptotriazine (DMT)] was obtained from Fisher Scientific; and farnesol, palladium (10%) on activated charcoal (Pd/C), anhydrous methanol, 2nd generation Grubbs' catalyst (Grubbs Catalyst M204), pyridine, dimethyl octanol, isoamyl alcohol, 4-dimethylaminopyridine (DMAP), N-(3-dimethylaminopropyl)-N-ethylcarbodiimide hydrochloride, and anhydrous dichloromethane were purchased from Sigma-Aldrich. Aluminum pans for SAXS and differential scanning calorimetry (DSC) were acquired from DSC Consumables, Inc. Deuterated chloroform and benzene- $d_6$  for  $^1$ H NMR spectroscopy were purchased from Cambridge Isotopes.

**Synthesis.** Synthesis of norbornene *exo,exo*-diester monomers, 3rd generation Grubbs' catalyst, homopolymers, and diblock polymers are described in detail in the Supporting Information. The polymers were produced by sequential ROMP and characterized by <sup>1</sup>H NMR spectroscopy and size-exclusion chromatography with multiangle light scattering (SEC-MALS) detection.

<sup>1</sup>H NMR Spectroscopy. Monomer and polymer chemical structural information were obtained by proton nuclear magnetic resonance (<sup>1</sup>H NMR) spectroscopy. <sup>1</sup>H NMR was also used to determine the volume fraction of the norbornene *exo,exo*-dimethyl ester block in each diblock polymer. <sup>1</sup>H NMR spectroscopy was performed on a Bruker Avance III Nanobay AX-400 spectrometer (400 MHz) with a 60-slot SampleXpress autosampler using 16, 64, or 128 scans. Monomers and polymers were characterized in deuterated chloroform, and 3rd generation Grubbs' catalyst in benzene-*d*<sub>6</sub>. Representative <sup>1</sup>H NMR spectra are provided in the Supporting Information.

**SEC-MALS.** SEC-MALS was performed using tetrahydrofuran (THF) as the mobile phase (1.0 mL/min) on an Agilent 1260 series instrument equipped with one Tosoh Styragel guard column and three successive Tosoh Styragel columns (G6000, G4000, and G2000) packed with rigid 5  $\mu$ m styrene-divinylbenzene particles. Polymer solutions were prepared at 4–6 mg/mL in uninhibited THF, and filtered with 0.22  $\mu$ m PTFE filters before injection. The polymer molecular characteristics—number-average molecular weight ( $M_{\rm m}$ ), weight-average molecular weight ( $M_{\rm m}$ ), and dispersity ( $D = M_{\rm w}/M_{\rm n}$ )—were determined using a Wyatt Technology DAWN Heleos II MALS detector with 658 nm wavelength light and a Wyatt OPTILAB T-rEX

refractive index (RI) detector operated at 25 °C. The RI increment  $(\partial n/\partial c)$  for each polymer was determined by the weight average of the measured  $\partial n/\partial c$  of the constituent homopolymers. Representative SEC plots of the diblock polymers are provided in the Supporting Information.

SAXS/MAXS/WAXS. Small-angle, mid-angle, and wide-angle X-ray scattering (SAXS, MAXS, and WAXS) experiments were performed at the Advanced Photon Source (APS) at Argonne National Laboratory, on the Sector 5-ID-D beamline of the Dupont-Northwestern-Dow Collaborative Access Team (DND-CAT). Bulk polymer samples (~10-20 mg) were loaded into aluminum Tzero DSC pans and hermetically sealed under argon. Before transport to APS, samples were annealed either at 140  $^{\circ}\text{C}$  for 24 h or at 200  $^{\circ}\text{C}$  for 1 h, then cooled to 180 °C for 2 h, then 160 °C for 3 h, and finally 140 °C for 20 h before cooling slowly to room temperature. During the experiment, samples were heated using a custom-fabricated 32-pan heating stage at 10 °C/min between temperatures, with a 15 min anneal at each temperature before measurement, over the temperature range 25-210 °C. Two-dimensional scattering patterns were collected with a 1 s exposure time and X-ray wavelength  $\lambda$  = 0.0729 nm. SAXS data were collected on a Rayonix MX170-HS detector and 8.5 m sample-to-detector distance, giving a wavevector q range of  $2.35 \times 10^{-3}$ – $0.192 \text{ Å}^{-1}$ . MAXS and WAXS data were collected on Rayonix LX170-HS CCD detectors with sample-todetector distances of 1.01 and 0.2 m, respectively, resulting in q ranges of  $0.13-0.86 \text{ Å}^{-1}$  for MAXS and  $0.68-4.5 \text{ Å}^{-1}$  for WAXS, where the magnitude of the scattering wavevector is given by  $q = 4\pi\lambda^{-1}\sin(\theta/2)$ , in which  $\theta$  is the scattering angle. To optimize the scattering signal and decrease noise, the detector readout was binned to 2 by 2 pixels.

SAXS and WAXS patterns were also collected at Sector 12-ID-B at the APS. Samples were loaded into standard DSC pans, hermetically sealed under argon, and pre-annealed as described above. Samples were heated using a custom fabricated 28-pan heating stage during the experiments, with the same protocol described above. Two-dimensional scattering patterns were collected with a 1 s exposure time and X-ray wavelength of  $\lambda=0.0886$  nm. The sample-to-detector distances were calibrated using silver behenate and gave SAXS q ranges of 2.24  $\times$  10<sup>-3</sup>–0.0896 Å<sup>-1</sup> and 3.84  $\times$  10<sup>-3</sup>–0.0884 Å<sup>-1</sup>, depending on the detector setting, and a WAXS q range of 0.82–2.23 Å<sup>-1</sup>. In both cases, the isotropic 2D data were averaged azimuthally to afford 1D scattering patterns as intensity versus q. The relative peak positions in the 1D patterns were indexed and assigned to different morphologies using IGOR Pro (WaveMetrics, Inc.) along with a SAXS indexing macro. <sup>30</sup>

SAOS Rheology. Small amplitude oscillatory shear (SAOS) experiments were performed on bulk homopolymers to determine the plateau modulus (G<sub>N</sub>) using a TA Instruments ARES-G2 rheometer equipped with a parallel plate geometry. Samples were loaded onto 8 or 25 mm diameter parallel plates and heated to 170 °C under nitrogen. Steady shear was applied for 5 min to aid in removing air bubbles from the sample. Strain sweeps were performed from 0.1 to 100% strain at various temperatures and 1 rad/s to identify the linear viscoelastic (LVE) regime where the storage (G') and loss (G'')moduli remain constant. Frequency sweeps were performed from 0.1 to 100 rad/s at temperatures ranging from -30 to +100 °C with applied strains from 1-10%, in the LVE regime. Van Gurp-Palmen plots and Gaussian chain analysis have been applied to determine G<sub>N</sub> and estimate the statistical segment lengths of the homopolymers. Further details about the analysis are provided in Supporting Information.

**DSC.** DSC measurements were performed on a TA Instruments Q1000. Approximately 2–8 mg of each sample was loaded into a hermetically sealed aluminum Tzero DSC pan. Samples were heated from 40 to 120 °C to erase any thermal history and then cooled to –120 °C and reheated to 120 °C at a ramp rate of 10 °C/min while sampling every 1 s. The data collected on the second heating were used to determine the glass transition temperature  $(T_{\rm g})$ . Representative DSC data can be found in the Supporting Information.

$$\begin{array}{c} \text{Mes-N} \\ \text{N-Ru} \\ \text{DCM, 25 °C} \\ \text{15 minutes} \\ \text{1 equiv.} \end{array}$$

Figure 1. Sequential ROMP synthetic scheme for the preparation of poly(norbornene exo,exo-dimethylester)-b-poly(norbornene exo,exo-dioligoPEP<sub>i</sub>).

#### RESULTS

To determine the effect of diblock polymer architectural asymmetry on self-assembly, with a focus on double gyroid phase formation, we synthesized five series of norbornenebased diblock copolymers, using sequential ROMP (Figure 1). All the diblocks contain a poly(norbornene exo,exo-dimethyl ester) (M) linear block, and the architectural asymmetry has been systematically raised by increasing the oligomeric poly(ethylene-alt-propylene) (oligo-PEP) side-chain length of the second polynorbornene-based block. As illustrated in Figure 1, the following second block types have been prepared: poly(norbornene exo,exo-di-isoamyl ester) (P<sub>1</sub>); poly-(norbornene exo,exo-di-3,7-dimethyloctyl ester) (P<sub>2</sub>); poly-(norbornene exo,exo-di-hexahydrofarnesyl ester) (P<sub>3</sub>); poly-(norbornene exo,exo-di-dihydrophytyl ester) (P<sub>4</sub>); and poly-(norbornene exo,exo-di-perhydrosolanesyl ester) ( $P_9$ ). The diblocks were designed to have relatively low glass transition temperatures  $(T_{\sigma})$  to broaden the temperature range over which the polymers can order. DSC measurements were performed with each of the constituent homopolymers and representative diblocks. DSC traces of the homopolymers show a distinct change in the slope of the heat flow curve, and a sharp peak in the derivative of the heat flow with respect to temperature, corresponding to the  $T_{\rm g}$  of the homopolymers (Figure S20). The  $T_{\sigma}$  for the M homopolymer was measured as  $\sim$ 70 °C (Figure S20a), while the values for  $P_1-P_9$  ranged between  $\sim -77$  and -40 °C (Figures S20b-f). DSC traces for the diblocks show two distinct  $T_g$ s, each  $T_g$  corresponding to the polymer constituting the diblocks (Figure S21).

Within each of the five sets of diblock polymers, the volumetric degree of polymerization (N) (for definition see footnote in Table 1) and the volume fraction of the M block  $(f_{\rm M})$  have been varied, resulting in a total of 223 polymers. The range of molecular weights  $(M_{\rm n})$ , dispersities (D),  $f_{\rm M}$ , and N, obtained for each of the diblock sets, are given in Table 1, where the ranges of  $f_{\rm M}$  have been chosen to capture the double gyroid phase window.

The thermotropic phase behavior of the diblock polymers was determined by SAXS over the temperature range 25–210 °C, both upon heating and cooling. Based on the morphologies obtained by SAXS at different temperatures (T), and using  $f_M$  and N values determined by  $^1\mathrm{H}$  NMR and SEC-MALS, phase portraits were generated for each polymer type, as displayed in Figure 2. Phase portraits are plotted as N/T as a function of  $f_M$ , where N/T is proportional to the segregation strength ( $\chi N$ ), where  $\chi$  is the Flory–Huggins interaction parameter, which is expected to be inversely proportional to temperature.  $^{31}$  As observed in Figure 2, all systems exhibit a double-gyroid phase

Table 1. Molecular Characteristics of Five Sets of Diblock Polymers  $^{a,e}$ 

polymer	$M_{\rm n}$ range $({ m kDa})^b$	$f_{\rm M}$ range <sup>c</sup>	N range <sup>d</sup>	<i>Đ</i> range <sup>b</sup>
$MP_1$	8.2-37.6	0.32 - 0.74	99-484	1.02 - 1.06
$MP_2$	9.4-22.1	0.36 - 0.72	118-287	1.01 - 1.05
$MP_3$	9.3-21.5	0.36 - 0.78	124-283	1.01 - 1.06
$MP_4$	6.9-21.8	0.36-0.55	91-289	1.02 - 1.07
$MP_9$	8.5-20.0	0.42 - 0.70	110-263	1.02 - 1.05

"For detailed characteristics of individual polymers, see the Supporting Information. <sup>b</sup>Molecular weight and dispersity were determined by SEC-MALS. 'Volume fraction of M determined by <sup>1</sup>H NMR spectroscopy. <sup>d</sup>Volumetric degree of polymerization estimated using the volume fraction and molecular weight  $N = [M_{\rm n}/(\rho_{\rm M}f_{\rm M} + \rho_{\rm P}f_{\rm P})] \cdot [N_{\rm av}v_{\rm ref}]^{-1}$ , where the densities of the constituent homopolymers  $(\rho)$  were determined at room temperature using a density determination kit from Mettler-Toledo Excellence XO/XS analytical balances, and  $N_{\rm av}$  and  $v_{\rm ref}$  are Avogadro's number and the reference volume of 118 ų, respectively. 'Data for MP₃, MP₄, and MP₂ block polymers are reproduced with permission from Liberman et al. <sup>28</sup> Copyright 2022 American Chemical Society.

and show the conventional transitions between hexagonally packed cylinders, double-gyroid, and lamellae with increasing  $f_{\rm M}$ . Representative examples of the 1D SAXS patterns for these morphologies are included in Figure 3a–c. Comparison of these phase portraits reveals that increasing architectural asymmetry expands the range of coexistence between different phases. While the least architecturally asymmetric diblock polymers, MP<sub>1</sub> (Figure 2a), mainly show the formation of pure phases, increasing the architectural asymmetry leads to broader windows of coexistence of double gyroid with hexagonally packed cylinders, lamellae, or both (Figure 2b–e). A representative 1D SAXS pattern displaying coexistence among all three phases is shown in Figure 3d. Possible sources of this phase coexistence are discussed below.

While all diblock families show double gyroid formation, the volume fractions and  $M_{\rm n}$  where the double gyroid window occurs vary with architectural asymmetry. Table 2 lists the ranges of  $M_{\rm n}$ ,  $f_{\rm M}$ , and N for the gyroid window, as well as the resulting gyroid domain spacings (d). Note that the maximum and minimum values reported in Table 2 are the molecular characteristics of the polymers that either self-assembled into pure gyroid or formed in coexistence with other phases. As architectural asymmetry increases, the maximum values, and the range of  $M_{\rm n}$  and N values, associated with the gyroid forming polymers decrease. Also evident is a shift toward lower N/T values of the gyroid window with increasing asymmetry, associated with an increasing  $\chi$ , resulting in limited or no access to the ODT. Restrictions on  $M_{\rm n}$  result in limitations on

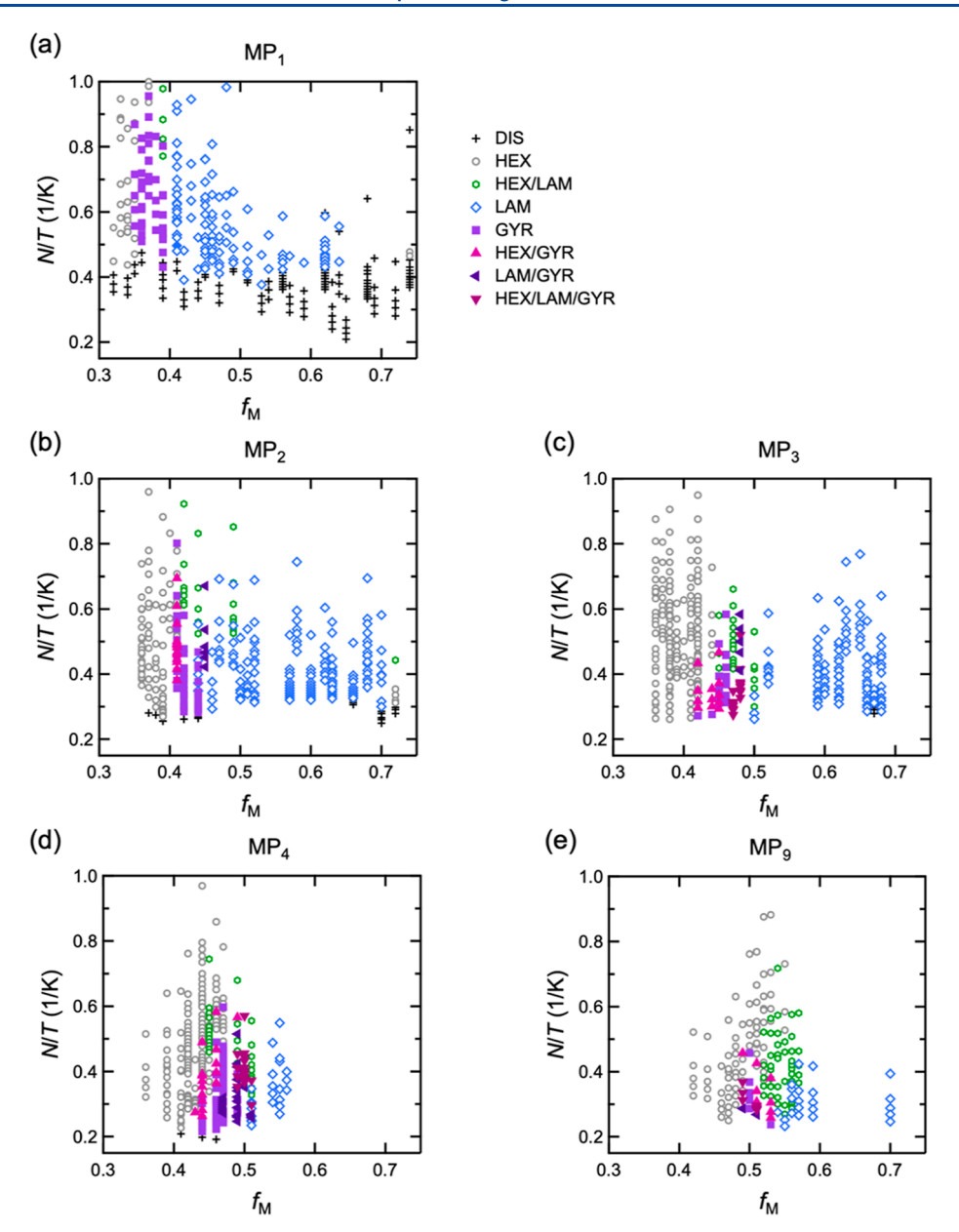


Figure 2. Phase maps plotted as N/T versus the volume fraction of the linear block,  $f_{M}$ , for (a)  $MP_1$ , (b)  $MP_2$ , (c)  $MP_3$ , (d)  $MP_4$ , and (e)  $MP_9$ , determined by SAXS. N and T refer to the volumetric degree of polymerization and the SAXS measurement temperature in Kelvin, respectively. DIS, HEX, GYR, and LAM in the legend denote disorder, hexagonally packed cylinders, double gyroid, and lamellae, respectively. Phase maps for  $MP_3$ ,  $MP_4$ , and  $MP_9$  are reproduced with permission from Liberman et al. Copyright 2022 American Chemical Society.

the accessible gyroid dimensions, as indicated by the range of d values listed in Table 2. Another observation from Figure 2 and Table 2 is that architectural asymmetry affects the location of the gyroid window, as well as its extent. With increasing asymmetry, the gyroid window shifts toward higher  $f_{\rm M}$  values. Additionally, the composition range of the gyroid window initially increases from  $\Delta f_{\rm M} = 0.04$  (for MP<sub>1</sub> and MP<sub>2</sub>) to 0.06 (for MP<sub>3</sub>), to 0.08 (for MP<sub>4</sub>), and then it narrows to 0.04 (for MP<sub>9</sub>).

**Linear-to-Bottlebrush Transition.** Bottlebrush polymers are defined as densely grafted polymers with a linear backbone, resulting in an extended backbone conformation.  $^{16,17}$  The transition from linear to bottlebrush polymers has been considered in terms of the average length of the backbone between grafts  $(L_{\rm g})$  and the length of the side chains  $(l_{\rm sc})$ .  $^{32-34}$  When  $L_{\rm g} > l_{\rm sc}$  the polymer is considered linear, with a

Gaussian coil behavior. However, when  $L_{\rm g} \ll l_{\rm sc}$  the polymer transitions into a bottlebrush, where the backbone accommodates an extended, wormlike configuration with different chain statistics and physical properties. In this work, the polymers have a polynorbornene backbone with a repeat unit contour length  $(L_{\rm c})$  of 6.2 Å, with a constant grafting density (z) of 2. The resulting backbone length between grafts can be estimated as  $L_{\rm g}=L_{\rm c}/2$ , which gives a constant  $L_{\rm g}=3.1$  Å, suggesting that polymers with  $l_{\rm sc}\gg 3.1$  Å may be considered as bottlebrushes.

To estimate  $l_{\rm sc}$ , we analyzed  $P_1$ ,  $P_2$ ,  $P_3$ ,  $P_4$ , and  $P_9$  homopolymers by MAXS and WAXS (Figure 4). The broad peak observed in the MAXS regime ( $q_{\rm bb} \cong 0.3~{\rm \AA}^{-1}$ ) for  $P_2$ ,  $P_3$ ,  $P_4$ , and  $P_9$ , corresponds to the average distance between backbones ( $d_{\rm bb} = 2\pi/q_{\rm bb}$ ), whereas the peak in the WAXS regime ( $q_{\rm sc} \cong 1.3~{\rm \AA}^{-1}$ ), correlates with the average distance

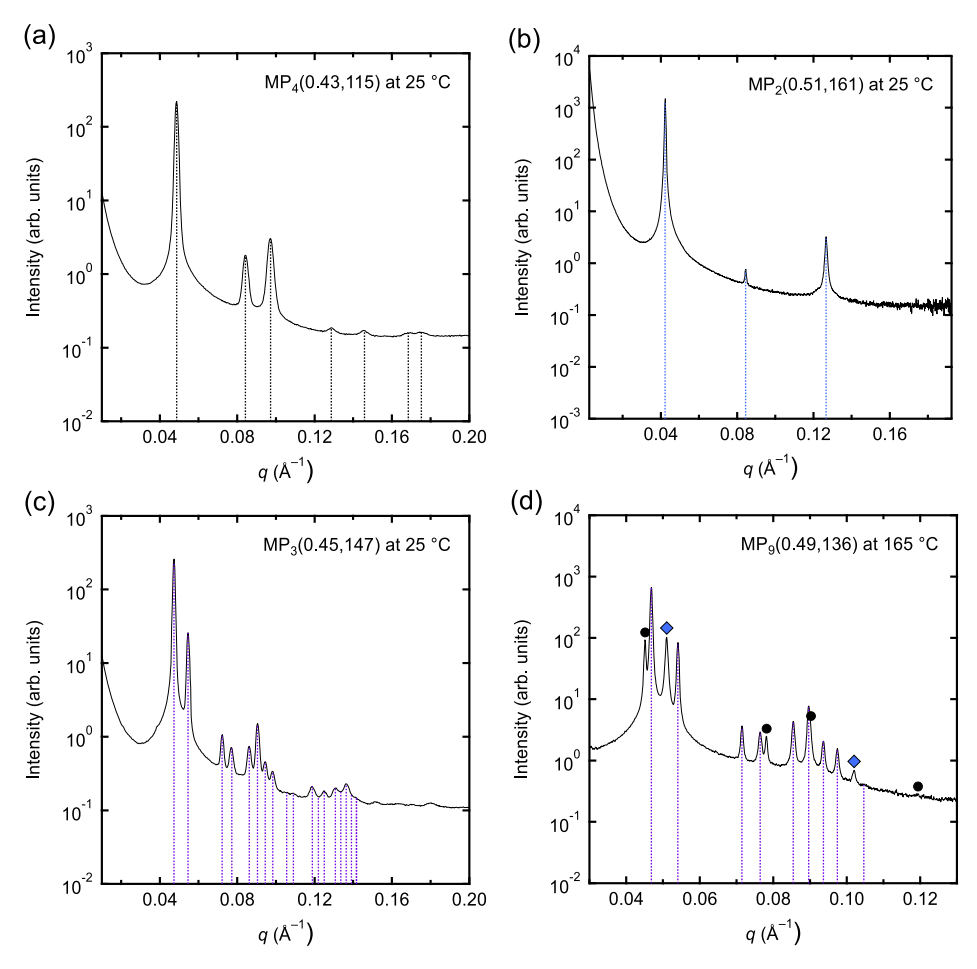


Figure 3. Representative SAXS patterns showing self-assembly into the following: (a) hexagonally packed cylinders for MP<sub>4</sub>( $f_M$ , N), (b) lamellae for MP<sub>2</sub>( $f_M$ , N), (c) double gyroid for MP<sub>3</sub>( $f_M$ , N), and (d) coexistence between hexagonally packed cylinders (black circles), lamellae (blue diamonds), and double gyroid (purple lines) phases for MP<sub>9</sub>( $f_M$ , N); vertical lines identify allowed reflections.

Table 2. Width of the Double Gyroid Phase Window

polymer	$M_{\mathrm{n}}$ range (kDa)	$f_{\rm M}$ range <sup>a</sup>	N range	d (Å) range
$MP_1$	12.4-25.5	0.35-0.39	159-329	130-224
$MP_2$	9.6-18.6	0.41 - 0.45	124-239	115-184
$MP_3$	9.8-13.4	0.42 - 0.48	129-174	113-165
$MP_4$	6.9-13.5	0.43 - 0.51	91-178	102-165
$MP_9$	8.7-10.3	0.49 - 0.53	113-136	127-137

"The ranges shown are based on the minimum and maximum values for polymers that formed the double gyroid phase, either pure or with phase coexistence.

between the oligo-PEP side chains ( $d_{\rm sc}=2\pi/q_{\rm sc}$ ).  $l_{\rm sc}$  can be estimated from  $d_{\rm bb}$ ; if there is no overlap between side chains,  $l_{\rm sc}=d_{\rm bb}/2$ , whereas if there is an intermolecular overlap,  $l_{\rm sc}>d_{\rm bb}/2$ . Table 3 summarizes the  $d_{\rm bb}$  and  $d_{\rm sc}$  values obtained by MAXS and WAXS for the homopolymers. Note that  $P_1$  did not generate a well-defined peak in the MAXS regime (Figure 4), suggesting there is not a well-defined distance between polymer backbones. If  $P_1$  is a Gaussian coil, it is plausible that it does not have a defined distance between chains. This suggests that  $P_1$  behaves as a flexible linear polymer. However,  $P_2$ ,  $P_3$ ,  $P_4$ , and  $P_9$  exhibit clearly defined  $q_{\rm bb}$  peaks, corresponding to increasing  $d_{\rm bb}$  of 22.0, 25.2, 28.5, and 36.6 Å, respectively. The associated values of  $d_{\rm bb}/2$ , presented in Table 3, are all significantly higher than  $L_{\rm g}=3.1$  Å. Even if there is some degree of overlap between the side chains, this

interpretation suggests that the P2 through P9 blocks can be considered as bottlebrushes, albeit with relatively short sidechain lengths. Moreover, the shift of  $q_{bb}$  toward lower q values (Figure 4), which results in an increase in  $d_{bb}$  with oligo-PEP side-chain length (Table 3), indicates that the self-concentration [SC] of the corresponding block increases. Selfconcentration is inversely related to the number of contacts between a given chain and other chains in the melt, captured by the ratio of the occupied versus pervaded volume of the polymer chain, such that [SC] = 1 for a solid sphere and  $[SC] \sim N^{-1/2}$  for a Gaussian coil.<sup>35</sup> Increasing the side-chain length increases [SC], which in turn leads to increasing architectural asymmetry in the MP<sub>i</sub> diblock polymers. This is in agreement with recent work by Chang and Bates<sup>12</sup> on linear-brush polymers, which demonstrated the consequences of increasing the [SC] of the brush block with side-chain length in selected diblock polymers. Another observation from Table 3 is a slight decrease in  $d_{sc}$  with the increase in side chain length, which might be due to the backbone becoming less flexible, on average. A stiffer backbone would result in a smaller mean inter-side-chain distance.

**Conformational Asymmetry Estimate.** Conformational asymmetry  $(\varepsilon)$  characterizes the difference between the volumes pervaded by the blocks through the statistical segment lengths (b):  $\varepsilon = (b_{\rm A}/b_{\rm B})$ , where  $b_{\rm i} = R_{\rm g}(6/N_{\rm i})^{1/2}$  and  $R_{\rm g}$  is the radius of gyration. Increasing the size of the side chain of the brush block changes its  $R_{\rm g}$  and therefore modifies b. The

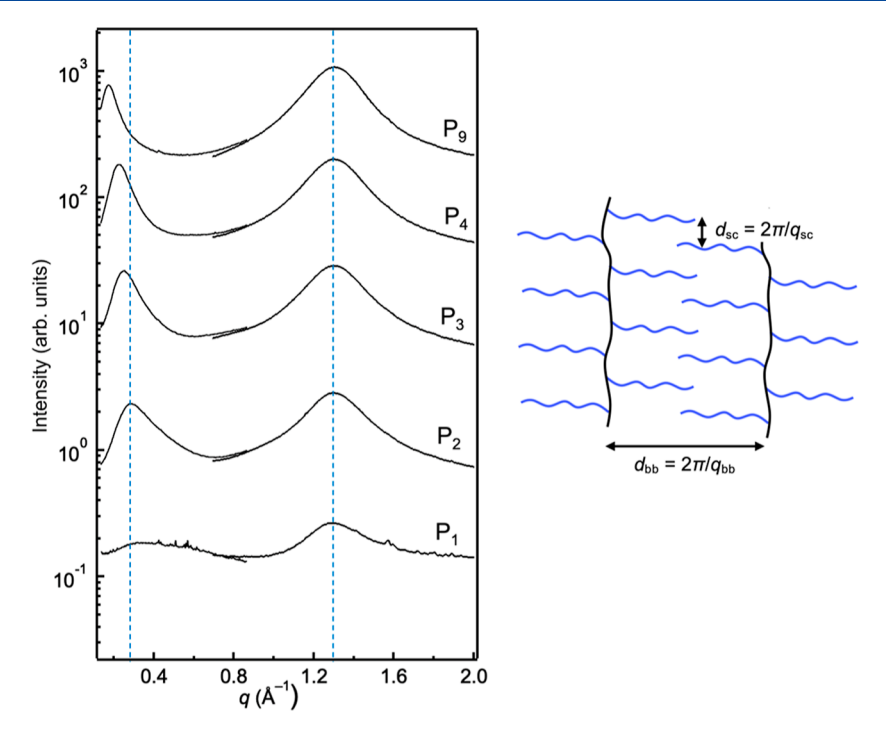


Figure 4. MAXS and WAXS data at obtained at 25 °C for  $P_1$ ,  $P_2$ ,  $P_3$ ,  $P_4$ , and  $P_9$  homopolymers. The peak observed at the lower q range for  $P_2$ ,  $P_3$ ,  $P_4$ , and  $P_9$  ( $q_{bb}$ ) corresponds to the average distance between backbones ( $d_{bb}$ ), and the peak at the higher q range ( $q_{sc}$ ) corresponds to the average distance between oligo-PEP side chains. Schematic illustration of the average  $d_{bb}$  and  $d_{sc}$  is presented on the right panel of the figure.

Table 3. Homopolymer Spatial Characteristics

homopolymer	$d_{\mathrm{bb}}  (\mathrm{\mathring{A}})^a$	$d_{\rm sc}  (\mathring{\rm A})^{b}$	$d_{\rm bb}/2~({\rm \AA})$
$\mathbf{P}_1$	not observed	$4.91 \pm 0.02$	
$P_2$	$22.0 \pm 0.1$	$4.85 \pm 0.02$	11.0
$P_3$	$25.2 \pm 0.1$	$4.84 \pm 0.02$	12.6
$P_4$	$28.5 \pm 0.5$	$4.83 \pm 0.01$	14.2
$P_9$	$36.6 \pm 0.5$	$4.82 \pm 0.01$	18.3

<sup>a</sup>Backbone distance from MAXS. <sup>b</sup>Side chain distance from WAXS.

statistical segment lengths for each of the constituent homopolymers were estimated from the plateau modulus  $(G_{\rm N})$  and normalized to a common reference volume ( $\nu_{\rm ref}$  = 118 Å<sup>3</sup>) to allow for comparison across systems.  $G_N$  values were determined using SAOS rheology as detailed in the Supporting Information. van Gurp-Palmen<sup>36</sup> plots were prepared for the homopolymers with phase angle  $(\delta)$  of the loss tangent versus complex modulus ( $|G^*|$ ) and are presented in Figure S22, and the estimated b values for each of the homopolymers are presented in Table S7. By increasing the side-chain length of the brush block,  $\varepsilon$  increases from 1.9, for MP<sub>1</sub>, to 4.8, for MP<sub>9</sub>. As noted in previous publications, <sup>1</sup> this analysis for estimating b from the plateau modulus pertains to Gaussian chains, and may not be strictly valid for bottlebrush-type chains. However, the obtained values should represent an internally consistent trend.

The increase in conformational asymmetry with side-chain length of the brush block, along with the increase in [SC] of the brush, which affects the free energy competition between chain stretching and interfacial area, both contribute to an increase in architectural asymmetry.

#### DISCUSSION

In this work, we synthesized five families of diblock polymers, varying the size of the side chain of the bottlebrush block ( $P_1$ ,

P<sub>2</sub>, P<sub>3</sub>, P<sub>4</sub>, and P<sub>9</sub>), the volume fraction of the linear (M) block, and overall degree of polymerization. We systematically studied how increasing the architectural asymmetry affects phase behavior, focusing primarily on the region in phase space near the double gyroid window. MAXS and WAXS measurements on P<sub>1</sub> to P<sub>9</sub> homopolymers demonstrate that the MP<sub>1</sub> is a linear-linear diblock, while MP<sub>2</sub>, MP<sub>3</sub>, MP<sub>4</sub>, and MP<sub>9</sub> are linear-bottlebrush diblocks, with with progressively increasing architectural asymmetry.

SAXS data acquired for the five sets of diblock polymers, and the corresponding phase maps, show that the polymers exhibit the conventional sequence of hexagonally packed cylinders to double gyroid to lamellar phases with increasing M block volume fraction. However, architectural asymmetry does affect the phase behavior. One effect is that as the diblocks transition from MP<sub>1</sub> to MP<sub>9</sub>, the polymers display greater regions of phase coexistence, rather than pure phases. Similar phase coexistence has also been found in our recent work on linearbottlebrush polymers.<sup>28</sup> However, when a pure block polymer self-assembles into an equilibrium morphology, regions of phase coexistence are not allowed, except precisely at a phase boundary. Therefore, the phase coexistence is either due to kinetic limitations, where the polymers are trapped in a nonequilibrium state, or due to dispersity. The phase maps reveal that the ODT becomes inaccessible with the increase in architectural asymmetry, indicative of an increase in the effective  $\chi$  parameter. Furthermore, upon closer examination of the sequence of morphologies formed by each block polymer at different temperatures (Tables S8-S12), it is evident that phase coexistence appears only when the block polymer does not have access to the ODT. Whenever a polymer does have access to the ODT, only pure phases are observed. An inaccessible ODT is indicative of relatively stronger segregation, which inhibits equilibration of kinetically trapped coexisting phases. When compared to the linear diblock

polymer, this behavior seems to be unique to the linear-brush polymer architecture. Previous studies show that even at high  $M_{\rm n}$ , strongly segregated linear block polymers microphase separate into pure phases.<sup>4,37</sup> This hypothesis could be explored by dissolving the diblocks in a good solvent, followed by solvent casting and annealing. Use of a solvent preferential for one block or the other may drive the morphology into different equilibrium or non-equilibrium states. Subsequent annealing will inform as to the kinetic constraints associated with metastable phases. On the other hand, the fact that the transition into the brush regime gives rise to phase coexistence might also indicate that the bottlebrush copolymer selfassembly is more sensitive to dispersity variations. Previous work by Park et al.<sup>38</sup> demonstrated that a linear diblock sample of polystyrene-b-polyisoprene with a narrow dispersity of 1.02 self-assembled into a pure hexagonally perforated layer morphology. However, once this polymer sample was fractionated into diblock fractions with 10% compositional variation, the individual specimens self-assembled into cylinders, double gyroid, or lamellae.<sup>38</sup> This shows that even a narrowly disperse polymer sample may contain a collection of macromolecules with a range of compositions, and once separated by composition, a variety of morphologies can be obtained. While the compositional variation usually does not produce phase coexistence in linear block polymers, we propose that the architectural asymmetry in linear-brush block polymers might lead to destabilization of pure phases, and to segregation into coexisting phases. This might be due to a sharper change in interfacial curvature at compositions between those associated with the hexagonally packed cylinders and lamellar phase boundaries.

Another observation from Figure 2 is that the location of the double gyroid window shifts to higher M block compositions with the increase in asymmetry. This is in qualitative agreement with theoretical work by Matsen<sup>11</sup> on architecturally asymmetric diblocks, as well as recent computational and experimental work that specifically focused on the linear-brush conformation. The shift in phase boundaries is rationalized by the spontaneous curvature toward the linear block induced by the architectural asymmetry, which favors the formation of morphologies with curved interfaces, such as cylinders and gyroid. The formation of lamellae would require higher volume fractions of the linear block to induce a flat interface between the two blocks.

The phase portraits in Figure 2 further demonstrate that the size of the gyroid window can be manipulated by the length of the side chain, whereby going from MP<sub>1</sub> to MP<sub>4</sub>, the gyroid window first increases in size, but then for MP9, it narrows again. However, in our recent publication,<sup>28</sup> we reported a similar polymer series comprising EP3, EP4, and EP9, where the pendant groups of the linear block were diethyl instead of dimethyl ester, and demonstrate that the gyroid window width, irrespective of the increasing architectural asymmetry, remains relatively constant. The apparent discrepancy between the two systems can be attributed to the interaction parameter. The phase diagrams shift to lower N/T values with architectural asymmetry, indicating an increase in segregation strength. This means that by increasing the side-chain length of the P<sub>i</sub> block,  $\chi$  gradually increases. When comparing between the phase maps of the  $EP_x^{28}$  and  $MP_x$  series, the shift toward lower N/Tvalues is stronger in the latter. This is further demonstrated by our estimates of  $\chi$  for the two systems in the previous work, where with the increase in architectural asymmetry, a steeper

increase in  $\chi$  is observed for MP<sub>x</sub>.<sup>28</sup> This stronger increase in  $\chi$  can cause a more prominent effect on the width of the gyroid window. Consistent with the trend observed in this study, previous theoretical studies in linear and architecturally asymmetric diblocks demonstrate that the segregation strength affects the size of the gyroid window, where it first increases in size, but then slightly narrows down again, after passing some optimal value where the gyroid window is the widest.<sup>9,11</sup>

#### SUMMARY

Through the well-controlled synthesis of five sets of diblock polymers, a total of 223 compounds, with a gradual increase in the length of the densely grafted side chains of the second block in each set, we have examined the impact of architectural asymmetry on the phase behavior of linear-bottlebrush polymers centered on the double gyroid network phase. MAXS analysis demonstrates that increasing the side-chain length of the bottlebrush block increases its self-concentration and results in a transition from a linear-linear to a linearbottlebrush conformation. SAXS data show that all five sets of materials exhibit the classical phases: hexagonally packed cylinders, double gyroid, and lamellae. Architectural asymmetry appears to induce phase coexistence, shifts the phase boundaries to higher compositions, and increases the apparent Flory-Huggins interaction parameter, all of which affect the location and extent of the double gyroid compositional window.

#### ASSOCIATED CONTENT

#### **Solution** Supporting Information

The Supporting Information is available free of charge at https://pubs.acs.org/doi/10.1021/acs.macromol.2c00758.

Detailed synthesis information, representative <sup>1</sup>H NMR spectra, SEC-MALS traces, DSC traces, SAXS patterns, and detailed diblock polymer characteristics (PDF)

#### AUTHOR INFORMATION

#### **Corresponding Authors**

Frank S. Bates — Department of Chemical Engineering & Materials Science, University of Minnesota, Minneapolis, Minnesota 55455, United States; orcid.org/0000-0003-3977-1278; Email: bates001@umn.edu

Timothy P. Lodge — Department of Chemical Engineering & Materials Science and Department of Chemistry, University of Minnesota, Minneapolis, Minnesota 55455, United States; orcid.org/0000-0001-5916-8834; Email: lodge@umn.edu

#### **Authors**

Lucy Liberman — Department of Chemical Engineering & Materials Science and Department of Chemistry, University of Minnesota, Minneapolis, Minnesota 55455, United States; orcid.org/0000-0001-9139-1163

McKenzie L. Coughlin – Department of Chemical Engineering & Materials Science, University of Minnesota, Minneapolis, Minnesota 55455, United States; orcid.org/ 0000-0001-9047-3319

Steven Weigand - Argonne National Laboratory, Lemont, Illinois 60439, United States

Jerrick Edmund – Department of Chemical Engineering & Materials Science, University of Minnesota, Minneapolis, Minnesota 55455, United States

Complete contact information is available at: https://pubs.acs.org/10.1021/acs.macromol.2c00758

#### **Author Contributions**

L.L. and M.L.C. authors contributed equally to this work.

#### Notes

The authors declare no competing financial interest.

#### ACKNOWLEDGMENTS

This work was supported by the National Science Foundation through the University of Minnesota MRSEC under award number DMR-2011401. Synchrotron SAXS experiments were performed at the 12-ID-B and 5-ID-D beamlines of the Advanced Photon Source (APS). This research used resources of the Advanced Photon Source, a U.S. Department of Energy (DOE) Office of Science User Facility operated for the DOE Office of Science by Argonne National Laboratory under contract no. DE-AC02-06CH11357. We thank Dr. Alice Chang for helpful advice and discussions, Dr. Aaron Lindsay for his help with collection of DSC data and fruitful discussions, and Camila Perales Rodriguez for help with sample preparation. M.L.C thanks the support of the National Science Foundation Graduate Research Fellowship Program under grant numbers 00039202 and 00074041.

#### REFERENCES

- (1) Li, L.; Schulte, L.; Clausen, L. D.; Hansen, K. M.; Jonsson, G. E.; Ndoni, S. Gyroid Nanoporous Membranes with Tunable Permeability. *ACS Nano* **2011**, *5*, 7754–7766.
- (2) Jo, G.; Ahn, H.; Park, M. J. Simple Route for Tuning the Morphology and Conductivity of Polymer Electrolytes: One End Functional Group Is Enough. ACS Macro Lett. 2013, 2, 990–995.
- (3) Dolan, J. A.; Wilts, B. D.; Vignolini, S.; Baumberg, J. J.; Steiner, U.; Wilkinson, T. D. Optical Properties of Gyroid Structured Materials: From Photonic Crystals to Metamaterials. *Adv. Opt. Mater.* **2015**, 3, 12–32.
- (4) Urbas, A. M.; Maldovan, M.; DeRege, P.; Thomas, E. L. Bicontinuous Cubic Block Copolymer Photonic Crystals. *Adv. Mater.* **2002**, *14*, 1850–1853.
- (5) Jackson, G. L.; Perroni, D. V.; Mahanthappa, M. K. Roles of Chemical Functionality and Pore Curvature in the Design of Nanoporous Proton Conductors. *J. Phys. Chem. B* **2017**, 121, 9429–9436.
- (6) Kim, H.; Leal, C. Cuboplexes: Topologically Active SiRNA Delivery. ACS Nano 2015, 9, 10214–10226.
- (7) Maldovan, M.; Urbas, A. M.; Yufa, N.; Carter, W. C.; Thomas, E. L. Photonic Properties of Bicontinuous Cubic Microphases. *Phys. Rev. B: Condens. Matter Mater. Phys.* **2002**, *65*, 165123.
- (8) Matsen, M. W.; Schick, M. Stable and Unstable Phases of a Diblock Copolymer Melt. *Phys. Rev. Lett.* **1994**, *72*, 2660–2663.
- (9) Cochran, E. W.; Garcia-Cervera, C. J.; Fredrickson, G. H. Stability of the Gyroid Phase in Diblock Copolymers at Strong Segregation. *Macromolecules* **2006**, *39*, 2449–2451.
- (10) Tyler, C. A.; Morse, D. C. Orthorhombic Fddd Network in Triblock and Diblock Copolymer Melts. *Phys. Rev. Lett.* **2005**, *94*, 208302
- (11) Matsen, M. W. Effect of Architecture on the Phase Behavior of AB-Type Block Copolymer Melts. *Macromolecules* **2012**, *45*, 2161–2165.
- (12) Chang, A. B.; Bates, F. S. Impact of Architectural Asymmetry on Frank-Kasper Phase Formation in Block Polymer Melts. *ACS Nano* **2020**, *14*, 11463–11472.
- (13) Park, S. J.; Cheong, G. K.; Bates, F. S.; Dorfman, K. D. Stability of the Double Gyroid Phase in Bottlebrush Diblock Copolymer Melts. *Macromolecules* **2021**, *54*, 9063–9070.

- (14) Grason, G. M.; Kamien, R. D. Interfaces in Diblocks: A Study of Miktoarm Star Copolymers. *Macromolecules* **2004**, *37*, 7371–7380.
- (15) Li, W.; Liu, Y. X. Simplicity in Mean-Field Phase Behavior of Two-Component Miktoarm Star Copolymers. J. Chem. Phys. 2021, 154, 014903.
- (16) Verduzco, R.; Li, X.; Pesek, S. L.; Stein, G. E. Structure, Function, Self-Assembly, and Applications of Bottlebrush Copolymers. *Chem. Soc. Rev.* **2015**, *44*, 2405–2420.
- (17) Pan, T.; Dutta, S.; Kamble, Y.; Patel, B. B.; Wade, M. A.; Rogers, S. A.; Diao, Y.; Guironnet, D.; Sing, C. E. Materials Design of Highly Branched Bottlebrush Polymers at the Intersection of Modeling, Synthesis, Processing, and Characterization. *Chem. Mater.* **2022**, *34*, 1990.
- (18) Xia, Y.; Kornfield, J. A.; Grubbs, R. H. Efficient Synthesis of Narrowly Dispersed Brush Polymers via Living Ring-Opening Metathesis Polymerization of Macromonomers. *Macromolecules* **2009**, *42*, 3761–3766.
- (19) Chang, A. B.; Lin, T.-P.; Thompson, N. B.; Luo, S.-X.; Liberman-Martin, A. L.; Chen, H.-Y.; Lee, B.; Grubbs, R. H. Design, Synthesis, and Self-Assembly of Polymers with Tailored Graft Distributions. *J. Am. Chem. Soc.* **2017**, *139*, 17683–17693.
- (20) Ruokolainen, J.; Saariaho, M.; Ikkala, O.; Ten Brinke, G.; Thomas, E. L.; Torkkeli, M.; Serimaa, R. Supramolecular Routes to Hierarchical Structures: Comb-Coil Diblock Copolymers Organized with Two Length Scales. *Macromolecules* 1999, 32, 1152–1158.
- (21) Brett Runge, M.; Lipscomb, C. E.; Ditzler, L. R.; Mahanthappa, M. K.; Tivanski, A. V.; Bowden, N. B. Investigation of the Assembly of Comb Block Copolymers in the Solid State. *Macromolecules* **2008**, *41*, 7687–7694.
- (22) Shin, S.; Moon, S.; Seo, M.; Kim, S. Y. Synthesis of Coil-Comb Block Copolymers Containing Polystyrene Coil and Poly(Methyl Methacrylate) Side Chains via Atom Transfer Radical Polymerization. *J. Polym. Sci., Part A: Polym. Chem.* **2016**, *54*, 2971–2983.
- (23) Wang, R.; Jiang, Z.; Yang, H.; Xue, G. Side Chain Effect on the Self-Assembly of Coil-Comb Copolymer by Self-Consistent Field Theory in Two Dimensions. *Polymer* **2013**, *54*, 7080–7087.
- (24) Watanabe, M.; Asai, Y.; Suzuki, J.; Takano, A.; Matsushita, Y. Frank-Kasper A15 Phase Formed in ABN Block-Graft Copolymers with Large Numbers of Graft Chains. *Macromolecules* **2020**, *53*, 10217–10224.
- (25) Mueller, A. J.; Lindsay, A. P.; Jayaraman, A.; Lodge, T. P.; Mahanthappa, M. K.; Bates, F. S. Quasicrystals and Their Approximants in a Crystalline-Amorphous Diblock Copolymer. *Macromolecules* **2021**, *54*, 2647–2660.
- (26) Nap, R. J.; Ten Brinke, G. Ordering at Two Length Scales in Comb-Coil Diblock Copolymers Consisting of Only Two Different Monomers. *Macromolecules* **2002**, *35*, 952–959.
- (27) Park, J.; Nam, J.; Seo, M.; Li, S. Side-Chain Density Driven Morphology Transition in Brush–Linear Diblock Copolymers. *ACS Macro Lett.* **2022**, *11*, 468–474.
- (28) Liberman, L.; Coughlin, M. L.; Weigand, S.; Bates, F. S.; Lodge, T. P. Phase Behavior of Linear-Bottlebrush Block Polymers. *Macromolecules* **2022**, *55*, 2821–2831.
- (29) Medrano, R.; Laguna, M. T. R.; Saiz, E.; Tarazona, M. P. Analysis of Copolymers of Styrene and Methyl Methacrylate Using Size Exclusion Chromatography with Multiple Detection. *Phys. Chem. Chem. Phys.* **2003**, *5*, 151–157.
- (30) Lindsay, A. P.; Mueller, A. J.; Mahanthappa, M. K.; Lodge, T. P.; Bates, F. S. 1D SAXS Indexing Macro for Igor Pro, 2021.
- (31) Bates, F. S.; Fredrickson, G. H. Block Copolymer Thermodynamics: Theory and Experiment. *Annu. Rev. Phys. Chem.* **1990**, *41*, 525–557.
- (32) Liang, H.; Cao, Z.; Wang, Z.; Sheiko, S. S.; Dobrynin, A. V. Combs and Bottlebrushes in a Melt. *Macromolecules* **2017**, *50*, 3430–3437.
- (33) Elli, S.; Ganazzoli, F.; Timoshenko, E. G.; Kuznetsov, Y. A.; Connolly, R. Size and Persistence Length of Molecular Bottle-Brushes by Monte Carlo Simulations. *J. Chem. Phys.* **2004**, *120*, 6257–6267.

- (34) Paturej, J.; Sheiko, S. S.; Panyukov, S.; Rubinstein, M. Molecular Structure of Bottlebrush Polymers in Melts. *Sci. Adv.* **2016**, 2, No. e1601478.
- (35) Rubinstein, M.; Colby, R. H. Polymer Physics; Oxford University Press: New York, 2003.
- (36) van Gurp, M.; Palmen, J. Time-Temperature Superposition for Polymer Blends. *J. Rheol. Bull.* **1998**, *64*, 5–8.
- (37) Politakos, N.; Ntoukas, E.; Avgeropoulos, A.; Krikorian, V.; Pate, B. D.; Thomas, E. L.; Hill, R. M. Strongly Segregated Cubic Microdomain Morphology Consistent with the Double Gyroid Phase in High Molecular Weight Diblock Copolymers of Polystyrene And. J. Polym. Sci., Part B: Polym. Phys. 2009, 47, 2419–2427.
- (38) Park, S.; Kwon, K.; Cho, D.; Lee, B.; Ree, M.; Chang, T. Phase Diagram Constructed from the HPLC Fractions of a Polystyrene-b-Polyisoprene Prepared by Anionic Polymerization. *Macromolecules* **2003**, *36*, 4662–4666.

### **□** Recommended by ACS

### Asymmetric Miktoarm Star Polymers as Polyester Thermoplastic Elastomers

Jacob R. Blankenship, Christopher M. Bates, et al.

JUNE 10, 2022 MACROMOLECULES

READ 🗹

#### Synthesis and Oxygen Permeation of Well-Defined Multistranded Copolymers from Monomers Having Two Different Polymerizable Groups

Yu Zang, Toshiki Aoi, et al.

JUNE 28, 2022 MACROMOLECULES

READ 🗹

### Nanobowls from Amphiphilic Core-Shell Cyclic Bottlebrush Polymers

Digvijayee Pal, Brent S. Sumerlin, et al.

AUGUST 22, 2022 MACROMOLECULES

READ 🗹

## **Self-Assembly of Molecular Brushes with Responsive Alternating Copolymer Side Chains**

Vitaly S. Kravchenko, Igor I. Potemkin, et al.

NOVEMBER 07, 2022

MACROMOLECULES

READ 🗹

Get More Suggestions >